A Tip of the Red Giant Branch Distance to the Dark Matter Deficient Galaxy NGC 1052-DF4 from Deep Hubble Space Telescope Data

Shany Danieli[1,2,3] , Pieter van Dokkum[3] , Roberto Abraham[4,5] , Charlie Conroy[6] , Andrew E. Dolphin[7,8] , and Aaron J. Romanowsky[9,10]

[1] Department of Physics, Yale University, New Haven, CT 06520, USA; shany.danieli@yale.edu, shanyi1@gmail.com
[2] Yale Center for Astronomy and Astrophysics, Yale University, New Haven, CT 06511, USA
[3] Department of Astronomy, Yale University, New Haven, CT 06511, USA
[4] Department of Astronomy and Astrophysics, University of Toronto, Toronto ON, M5S 3H4, Canada
[5] Dunlap Institute for Astronomy and Astrophysics, University of Toronto, Toronto ON, M5S 3H4, Canada
[6] Harvard-Smithsonian Center for Astrophysics, 60 Garden Street, Cambridge, MA, USA
[7] Raytheon, 1151 E. Hermans Road, Tuscon, AZ 85706, USA
[8] Steward Observatory, University of Arizona, 933 North Cherry Avenue, Tucson, AZ 85721-0065, USA
[9] Department of Physics and Astronomy, San José State University, San Jose, CA 95192, USA
[10] University of California Observatories, 1156 High Street, Santa Cruz, CA 95064, USA
Received 2019 October 16; revised 2020 April 24; accepted 2020 April 24; published 2020 May 15

Abstract

Previous studies have shown that the large, diffuse galaxies NGC 1052-DF2 and NGC 1052-DF4 both have populations of unusually luminous globular clusters as well as a very low dark matter content. Here we present newly obtained deep Hubble Space Telescope Advanced Camera for Surveys imaging of one of these galaxies, NGC 1052-DF4. We use these data to measure the distance of the galaxy from the location of the tip of the red giant branch (TRGB). We find a rapid increase in the number of detected stars fainter than $m_{F814W} \sim 27.3$, which we identify as the onset of the red giant branch. Using a forward modeling approach that takes the photometric uncertainties into account, we find a TRGB magnitude of $m_{F814W,TRGB} = 27.47 \pm 0.16$. The inferred distance, including the uncertainty in the absolute calibration, is $D_{TRGB} = 20.0 \pm 1.6$ Mpc. The TRGB distance of NGC 1052-DF4 is consistent with the previously determined surface brightness fluctuation distance of $D_{SBF} = 18.7 \pm 1.7$ Mpc to NGC 1052-DF2 and is consistent with the distance of the bright elliptical galaxy NGC 1052. We conclude that the unusual properties of these galaxies cannot be explained by distance errors.

1. Introduction

In 2016, as part of the Dragonfly Nearby Galaxies Survey (Merritt et al. 2016), we identified 23 low surface brightness galaxies in four survey fields: NGC 1052, NGC 1084, M 96, and NGC 4258. Follow-up Hubble Space Telescope (HST)/ Advanced Camera for Surveys (ACS) observations (Cohen et al. 2018) revealed that two of these galaxies, NGC 1052-DF2 and NGC 1052-DF4, in the field of the elliptical galaxy NGC 1052, have unusual properties with respect to the rest of the sample. At the distance of NGC 1052 ($D_{1052} = 19.4$–21.4 Mpc; Tonry et al. 2001; Blakeslee et al. 2002), NGC 1052-DF2 and NGC 1052-DF4 have the stellar masses of dwarf galaxies ($\sim 2 \times 10^8\, M_\odot$ and $\sim 1.5 \times 10^8\, M_\odot$, respectively) but large sizes ($R_e = 2.2$ and 1.6 kpc). Furthermore, they both host a spectacular population of luminous globular clusters. The specific frequency and median luminosity of the clusters are much higher than seen in other galaxies with the same stellar mass (van Dokkum et al. 2018a, 2019a).

Unusual as these aspects are, their kinematics turned out to be even more surprising. In 2018 we found that NGC 1052-DF2 seems to be lacking in dark matter (van Dokkum et al. 2018c), based on the radial velocities of 10 of its globular clusters. The inferred velocity dispersion of the galaxy is $\sigma_{gc} = 7.8^{+5.2}_{-2.2}$ km s^{-1} (van Dokkum et al. 2018b). Some studies raised concerns about these results, largely due to the small number of tracers (Martin et al. 2018; Laporte et al. 2019).

Follow-up spectroscopy of the diffuse stellar light with the Keck Cosmic Web Imager (KCWI) and the Multi-Unit Spectroscopic Explorer confirmed the low dispersion of NGC 1052-DF2 (Danieli et al. 2019; Emsellem et al. 2019). In particular, the high resolution KCWI data gave $\sigma_{stars} = 8.5^{+2.3}_{-3.1}$ km s^{-1}, fully consistent with the results inferred from the globular clusters (Danieli et al. 2019). Similarly, NGC 1052-DF4 has an inferred velocity dispersion of $\sigma_{gc} = 4.2^{+4.4}_{-2.2}$ km s^{-1} based on seven globular clusters (van Dokkum et al. 2019a), consistent with the expected value from the stars alone (7 km s^{-1}). Given the spatial extent of these galaxies, we do not expect them to be baryon-dominated within the effective radius (see, e.g., van Dokkum et al. 2019c). The two galaxies share essentially all their anomalous properties: they have similar sizes, luminosities, and colors; the same morphology; they both have a population of luminous globular clusters; and they both have a velocity dispersion that is consistent with that expected from the stellar mass alone.

Many of the unusual properties of NGC 1052-DF2 and NGC 1052-DF4 are distance-dependent, and accurate constraints on the dark matter content and the globular cluster luminosity function require accurate distances. The canonical distance to both galaxies is ~19 Mpc, based on their radial velocities, their presumed membership of the NGC 1052 group, and a surface brightness fluctuation (SBF) measurement from the then-available 2-orbit (1 orbit F814W and 1 orbit F606W) HST data (Blakeslee & Cantiello 2018; Cohen et al. 2018; van

Dokkum et al. 2018d). In particular, van Dokkum et al. (2018d) use a megamaser-TRGB-SBF distance ladder that is free of calibration uncertainties to determine a distance of $D_{\mathrm{SBF}} = 18.7 \pm 1.7$ Mpc to NGC 1052-DF2. However, others have suggested that the galaxies are significantly closer to us. Trujillo et al. (2019) and Monelli & Trujillo (2019) derive distances of ≈ 13 and 14.2 ± 0.7 Mpc to NGC 1052-DF2 and NGC 1052-DF4, respectively, from the same HST imaging. In contrast to van Dokkum et al. (2018d). They associate faint detections in the HST data with individual stars on the red giant branch, and associate the brightest of these detections with the tip of the red giant branch (TRGB). A shorter distance would bring NGC 1052-DF2 and NGC 1052-DF4 more in line with other galaxies: their physical sizes would be smaller, their globular clusters less luminous, and their mass-to-light ratios slightly higher.[11]

These disagreements can be resolved using deeper data. The previously available 1+1 orbit HST data are not deep enough to detect the TRGB beyond $D \sim 15$ Mpc, and the color–magnitude distributions (CMDs) generated by the two studies are highly sensitive to the quality cuts that are applied to the photometry. In this Letter we present significantly deeper HST/ACS observations of NGC 1052-DF4, obtained in a Cycle 26 midcycle program. Using a total of 8 orbits in F814W and 4 orbits in F606W we measure the distance to the galaxy based on a secure determination of the TRGB magnitude. Vega magnitudes are used throughout this paper.

2. HST/ACS Observations and Processing

NGC 1052-DF4 was observed with the HST ACS Wide-Field Channel (WFC) in Cycle 26 midcycle program 15695 in July 2019 in three visits. We obtained seven orbits in the F814W filter and three orbits in the F606W filter. Adding these data to the observations that we obtained in 2017 (program 14644), the total exposure time is 16,760 s in F814W and 8240 s in F606W. The pointing and orientation were constrained to ensure that the neighboring galaxy NGC 1052-DF5 (with a projected distance of $\sim 90''$ from NGC 1052-DF4) would be included in the field of view. NGC 1052-DF4 was placed near the center of one of the WFC chips.

The observations were obtained with a standard dither pattern with four exposures in each orbit to optimally sample the point-spread function and to facilitate the identification of hot pixels and cosmic rays. Individual exposures were bias-subtracted and dark-current-subtracted, flat-fielded, and CTE-corrected by the STScI pipeline, providing calibrated `flc` files. We used the `TweakReg` utility to align the 48 `flc` files and AstroDrizzle to combine the aligned `flc` images into astrometrically corrected drizzled images (`drc`) in the F814W and F606W filters.

A color image of NGC 1052-DF4, generated from the drizzled images, is shown in Figure 1. As can be seen in the zoomed-in panel, the galaxy is well-resolved into stars in these deep data. The red giants appear as thousands of yellow point sources against a bluer unresolved backdrop of subgiants and main-sequence stars. The much-fainter neighboring galaxy NGC 1052-DF5 is not shown, but we note here that it is also resolved into stars: approximately 200 giants are detected down

to $m_{\mathrm{F814W}} < 28$ mag within two effective radii (with R_e from Cohen et al. 2018). This enigmatic object is the topic of a future paper.

3. Stellar Photometry

Photometry was carried out on the bias-subtracted, flat-fielded, CTE-corrected `flc` images, produced by the STScI ACS pipeline. We used the software package DOLPHOT,[12] which is a modified version of HSTphot (Dolphin 2000). The DOLPHOT/ACS package includes a sequence of image preparation steps that are performed prior to the detection of stars. These include masking of bad columns and hot pixels (`acsmask`) and background determination using the `calcsky` module. These preprocessing steps were run on the 48 `flc` files as well as on the chosen reference `drc` image (the deepest drizzled image was chosen with 32 stacked `flc` images in F814W and a total exposure time of 16,760 s).

DOLPHOT detects stars by fitting PSFs generated with Tiny Tim (Krist 1995) simultaneously to all 48 `flc` images. This approach has the advantage that no resampling of the data is required and the noise properties of the observations are conserved. After detection in the full stack the software measures fluxes separately in the F814W and F606W frames. The three DOLPHOT parameters that have the strongest influence on the photometry are the sky fitting parameter (`FitSky`), the aperture radius (`RAper`), and the `Force1` parameter that forces all sources detected to be fitted as stars. We adopted the following: `FitSky`=2, `RAper`=3, and `Force1`=1. Those are similar to the recommended parameters on the DOLPHOT website, those used in the ANGST survey (Dalcanton et al. 2009), and in the GHOSTS project (Radburn-Smith et al. 2011) and optimize the photometry for cases of crowded stellar fields. As discussed in Section 4.3, with these parameters we find a systematic error of 0.1 mag at $m_{\mathrm{F814W}} = 27.0$ in the recovered magnitudes of artificial stars.

The raw DOLPHOT output was corrected for Galactic extinction of 0.041 mag in F814W and 0.066 mag in F606W (Schlafly & Finkbeiner 2011), and filtered to isolate stars with reliable photometry. Only objects with signal-to-noise ratio >4 in F814W, signal-to-noise ratio >2 in F606W, object-type $\leqslant 2$ (that is, good star or faint star), $|\mathrm{sharp}_{\mathrm{F814W}}| \leqslant 0.5$, $|\mathrm{sharp}_{\mathrm{F606W}}| \leqslant 0.5$, $\mathrm{crowd}_{\mathrm{F814W}} \leqslant 0.5$, and $\mathrm{crowd}_{\mathrm{F606W}} \leqslant 0.5$ were retained. We also obtained photometry of 200,000 artificial stars uniformly covering the magnitude and color ranges $25 < \mathrm{F814W} < 29$ and $1 < \mathrm{F606W} - \mathrm{F814W} < 1.5$. Furthermore, the stars were distributed between R_{eff} and $4R_{\mathrm{eff}}$, i.e., excluding the central part of the galaxy where crowding is most severe. Stars were injected at random positions out to four effective radii into the `flc` frames, and treated in exactly the same way as the actual photometry.

In Figure 2 we show examples of stellar detections of small regions in the center and in the outskirts of the galaxy. With the new deep HST images, the signal-to-noise is just high enough to obtain photometry of stars down to $m_{\mathrm{F814W}} \approx 28$ mag (see Section 4 for the uncertainty as a function of magnitude). In the central regions many objects are rejected as they are blended. In the outskirts we find a large population of unblended stars.

---

[11] A short distance is not without problems: the radial velocities of the galaxies, their SBF signal, and their apparent isolation in the foreground of the NGC 1052 group would all require explanations.
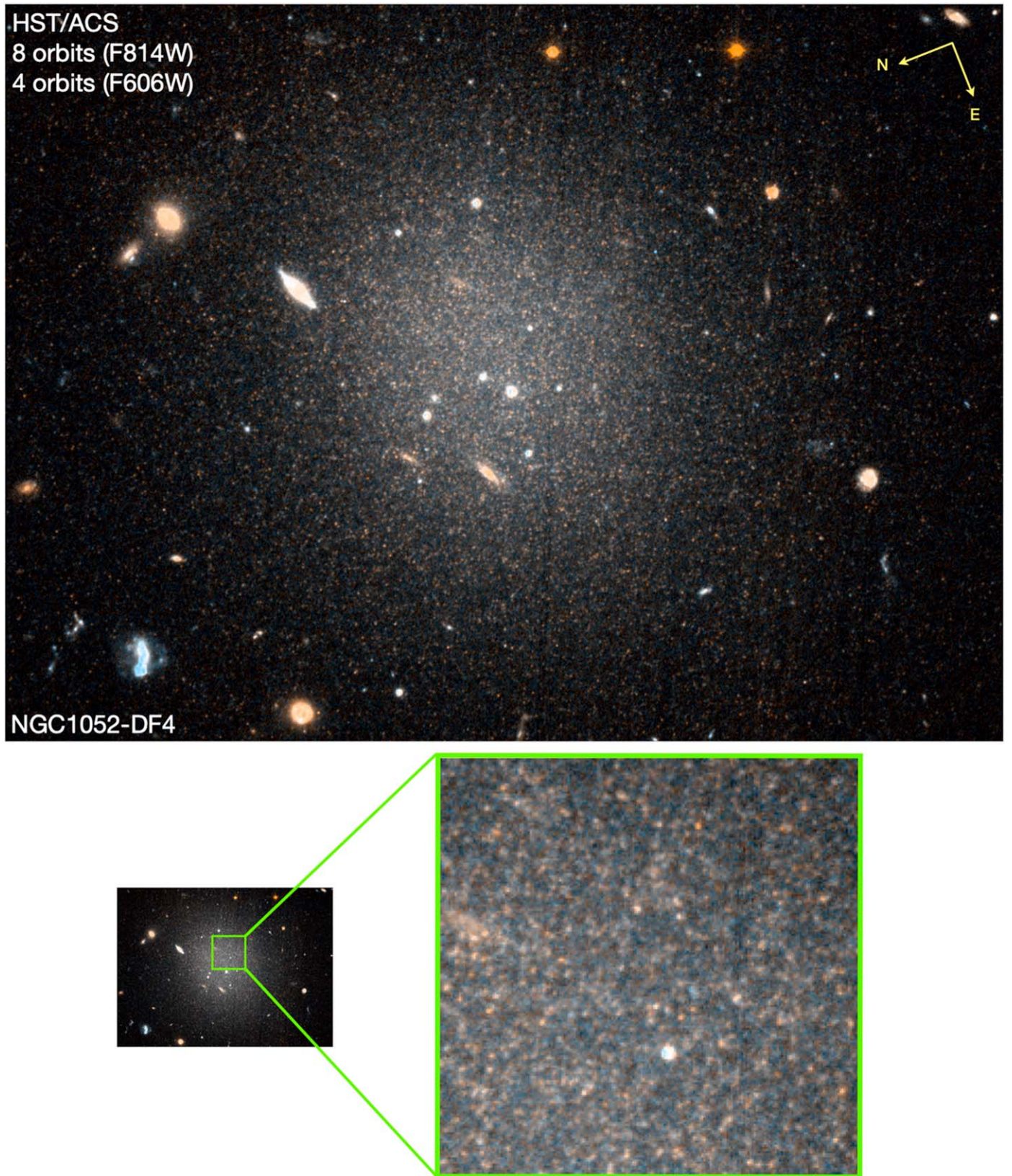
[12] http://americano.dolphinsim.com/dolphot/

Figure 1. Deep HST image of NGC 1052-DF4 obtained with the ACS. The total exposure time is 16,760 s (eight orbits) in the F814W filter and 8240 s (four orbits) in the F606W filter. The bottom panel shows a zoom on the central region of the galaxy. The image reveals a resolved red giant branch against the glow of unresolved bluer subgiants and main-sequence stars.
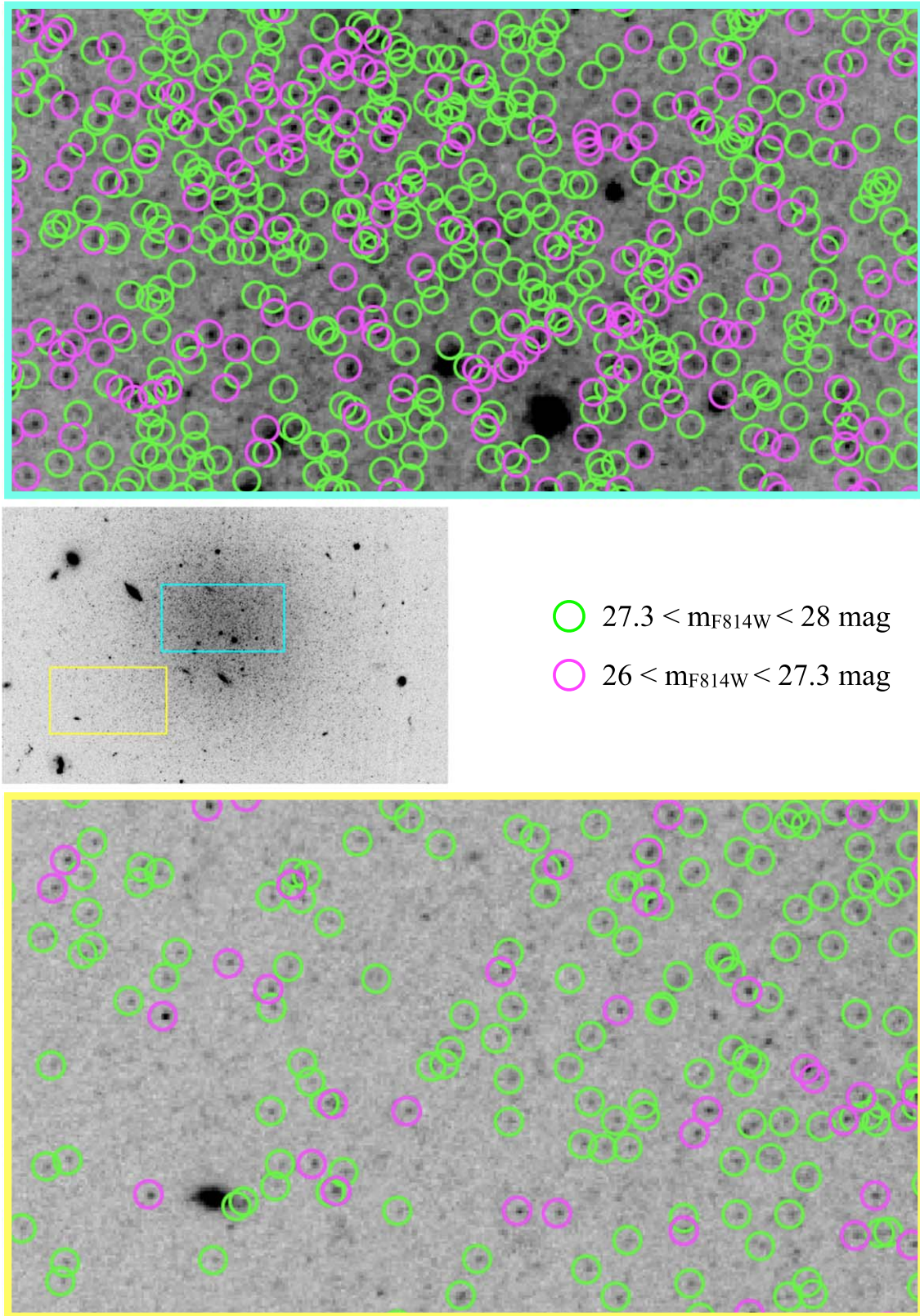
$27.3 < m_{F814W} < 28$ mag

$26 < m_{F814W} < 27.3$ mag

Figure 2. Detected stars (after quality cuts) from the stellar photometry catalog, shown in small regions in the outskirts (yellow) and in the center (cyan) of NGC 1052-DF4. RGB stars with $27.3 < m_{F814W} < 28$ mag are circled in green and likely AGB stars with $26 < m_{F814W} < 27.3$ mag in magenta. Note that many objects do not survive the quality cuts, particularly in the center where blends dominate over isolated stars. Stars in the central part of the galaxy ($R < R_{eff}$) are excluded from the TRGB measurement.
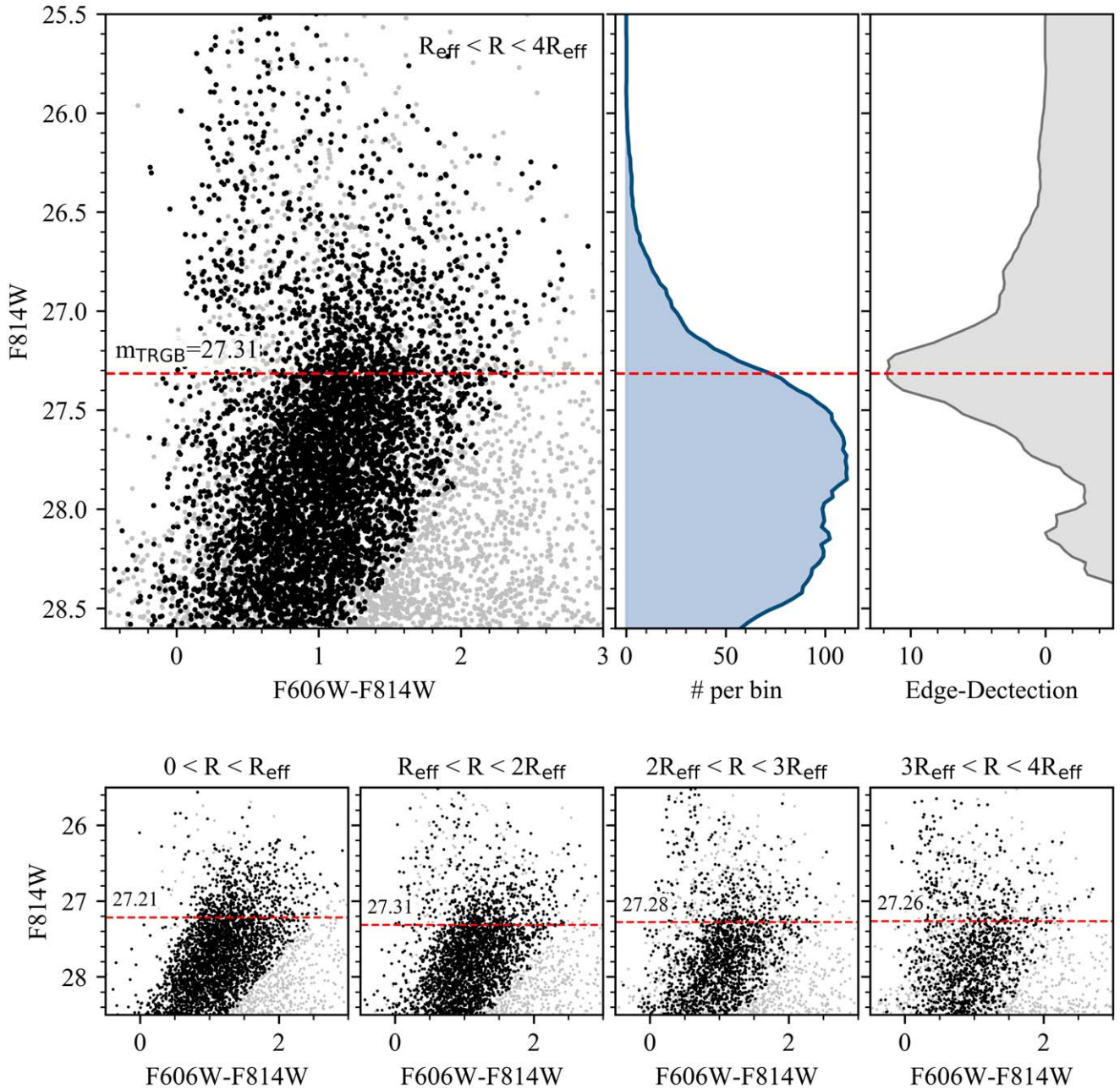
Figure 3. TRGB edge detection for NGC 1052-DF4. Top panels: the color–magnitude diagram (left), the binned luminosity function in F814W in 0.03 mag intervals (middle) and the response function of the $[-1, 0, +1]$ kernel on the smoothed luminosity function, for stars within the radial bin $R_{eff} < R < 4R_{eff}$. The location of the measured TRGB magnitude is marked with the dashed red line where we measure an F814W TRGB magnitude of $m_{F814W,TRGB} = 27.31 \pm 0.10$ mag. Bottom panels: the color–magnitude diagrams for various radial bins with the corresponding measured TRGB magnitude shown with the dashed red line. Black points show detected point sources remaining after applying quality cuts and light gray points show all detections before applying quality and color cuts to the photometry.

4. Distance from the TRGB

4.1. CMDs

CMDs for different radial bins are shown in the main panel and the bottom panels of Figure 3. The CMDs show the characteristic color–magnitude trend of the bright end of the RGB (see, e.g., Makarov et al. 2006; Hatt et al. 2018). The scatter is driven by the large uncertainties in the F606W magnitudes: the stars are red, and the exposure time in F606W is only half that in F814W. These color uncertainties do not affect the F814W luminosity function, which is used to derive the distance. There is a characteristic increase in the number of stars fainter than $m_{F814W} \sim 27.3$ mag, which we identify as the

onset of the red giant branch, i.e., the TRGB. This increase is illustrated by the difference between the number of magenta and green circles in Figure 2.

The TRGB marks the core helium flash of first-ascent red giant branch stars. Observationally, this physical phenomenon causes a sharp cutoff of the bright end of the red giant branch luminosity function, located at $M_{I,TRGB} \approx -4.0$. In the following sections we describe the determination of the TRGB magnitude and the associated distance using two methods: a standard edge detection and forward modeling of the F814W-band stellar luminosity function of the galaxy.

4.2. Edge Detection

The edge-detection method measures the first-derivative of a finely binned and smoothed luminosity function of the RGB and AGB populations. Briefly, a modified Sobel kernel, [−1, 0, +1], is used as a filter and is applied to the Gaussian-smoothed (with a smoothing scale of 0.25 mag) F814W-band luminosity function. When photometric errors are small the method returns a maximum response at the location of the TRGB, where the slope of the luminosity function reaches a global maximum. The peak in the filtered luminosity function is fitted with a Gaussian to determine its location and width. The method has been used widely (e.g., Lee et al. 1993; Caldwell 2006; Peacock et al. 2015; Sand et al. 2015; Hatt et al. 2018; Müller et al. 2018; Beaton et al. 2019).

Figure 3 shows the results of the TRGB measurement using the edge-detection method. The main result was determined from a sample in the radial range $R_{\rm eff} < R < 4R_{\rm eff}$ (upper panel), with the quality cuts of Section 3. Blue stars with (F814W − 28) + 1.5 × (F606W − F814W) > 0.5 are omitted. We measure an F814W TRGB magnitude of $m_{\rm F814W,\,TRGB} = 27.31 \pm 0.10$ mag for NGC 1052-DF4, where the uncertainty is taken as the width of the Gaussian fit to the peak. The bottom panel of Figure 3 shows results from other radial bins. The results are consistent for all radial bins including the innermost one $(0 < R < R_{\rm eff})$, where the data are severely crowded and most of the initial DOLPHOT detections are rejected by the quality cuts. This validates the quality cuts that are applied to the photometry and their ability to minimize crowding effects.

The uncertainty does not include systematic errors due to photometric errors or the calibration of the TRGB magnitude. As we show in Section 4.3, these uncertainties have a significant effect on the location of the TRGB.

4.3. Forward Modeling

Photometric errors take three forms: systematic errors ("bias"), scatter, and incompleteness. Following previous studies (e.g., Dalcanton et al. 2012; Geha et al. 2015; Conroy et al. 2018; Bennet et al. 2019) we quantify all three aspects using the photometry of artificial stars (see Section 3). The results are shown in Figure 4. Bright stars are recovered without bias and with very small scatter, but the errors gradually rise toward fainter magnitudes. At $m_{\rm F814W} = 27.0$ the recovered magnitudes are systematically 0.10 mag fainter than the input magnitudes, the 1σ scatter is 0.12 mag, and the completeness, determined from the ratio of the output magnitude distribution to the input magnitude distribution, is 92%. These artificial star test results are quantified with fifth-order polynomial fits, shown by the solid lines.

With the errors thus parameterized we determine the TRGB distance through a forward modeling procedure, as follows. First, a fully populated model for the galaxy is generated. Stars are drawn stochastically from a MIST isochrone (Choi et al. 2016; Dotter 2016) with an age of 10 Gyr and a metallicity [Fe/H] = −1, to match the color of the integrated stellar population as measured from the HST images. The results are not sensitive to the exact choice of stellar population parameters. The model contains 10^9 stars down to $M_{\rm F814W} = 11.3$ mag. For an assumed TRGB magnitude a model observed F814W-band magnitude distribution is calculated, down to $m_{\rm F814W} = 30$ mag. Next, observational

errors are applied to the model by shifting the brightness of each star by the parameterized bias, perturbing it by a random number drawn from a Gaussian distribution with a width that is given by the parameterized scatter. Possible mismatch between the number of AGB stars in the model and the true number, as well as contamination by blends, field stars, compact galaxies, and noise is taken into account with a linear function of the form $N_{\rm contam} = 20c \times (m - 26)$ for $m > 26$, and $N_{\rm contam} = 0$ for $m < 26$, with c a fit parameter. $N_{\rm contam}$ is added to the model and the observed brightness function is multiplied by the completeness. Each model is therefore characterized by two parameters, $m_{\rm F814W,TRGB}$ and c, and we determine the best-fitting values for these parameters by minimizing χ^2. The method is similar to that employed in the TRGBTOOL (Makarov et al. 2006), but with fewer free parameters.[13] We note that our fitting method is independent of the absolute calibration of the MIST models: we do not fit directly for a distance but we fit for the location of the discontinuity in the apparent magnitude distribution. This TRGB location is then converted into a distance modulus using the standard calibration in this field (see below).

We perform the fit on the F814W luminosity function at $R_{\rm eff} < R < 4R_{\rm eff}$, with 50 magnitude bins between 25.50 and 27.85 mag. The best fit is obtained for a TRGB magnitude of $m_{\rm F814W,TRGB} = 27.47^{+0.04}_{-0.02} \pm 0.16$, where the first error is statistical and the second is systematic. The reduced χ^2 of the best fit is 0.98. The statistical uncertainty encompasses 68% of the likelihood function (marginalized over c) from the forward modeling fitting. The main source of systematic uncertainty is that we strongly rely on the results of the artificial star tests due to our relatively low signal-to-noise ratio (compared to studies of galaxies that are much closer). The artificial stars show that both the magnitude bias and the photometric scatter are 0.15 mag near the TRGB location. This bias and scatter are taken into account in our forward modeling, but we conservatively assign a 0.15 mag systematic uncertainty to our TRGB measurement. Additionally, we find that varying the fitting range and the quality cuts to the photometry lead to ±0.04 mag variations in the measured TRGB magnitude. The final systematic uncertainty of 0.16 mag is the quadratic sum of these two contributions.

The best-fitting model is shown in Figure 4, both before ("intrinsic model") and after applying the photometric errors. The derived TRGB magnitude is fainter than that determined from the edge detection (see above). The reason is the photometric scatter, which has a larger effect on the apparent location of the TRGB than the photometric bias: due to the steepness of the luminosity function the number of stars that scatter from faint to bright magnitudes is much larger than that scattering from bright to faint magnitudes.

The absolute magnitude of the TRGB in the F814W-band is taken from the calibration of Rizzi et al. (2007). Their zero-point calibration of the TRGB is color-dependent, and accounts for shifts in the TRGB location due to variation in metallicity and age:

$$M_{\rm F814W}^{\rm ACS} = -4.06 + 0.20[(F606W - F814W) - 1.23]. \quad (1)$$

Using a TRGB median color index of 1.35 mag, we derive a TRGB absolute magnitude of $M_{\rm F814W} = -4.036$ mag. We

---

[13] The TRGBTOOL has four free parameters: the distance, the slope of the counts on each side of the TRGB, and the strength of the TRGB.
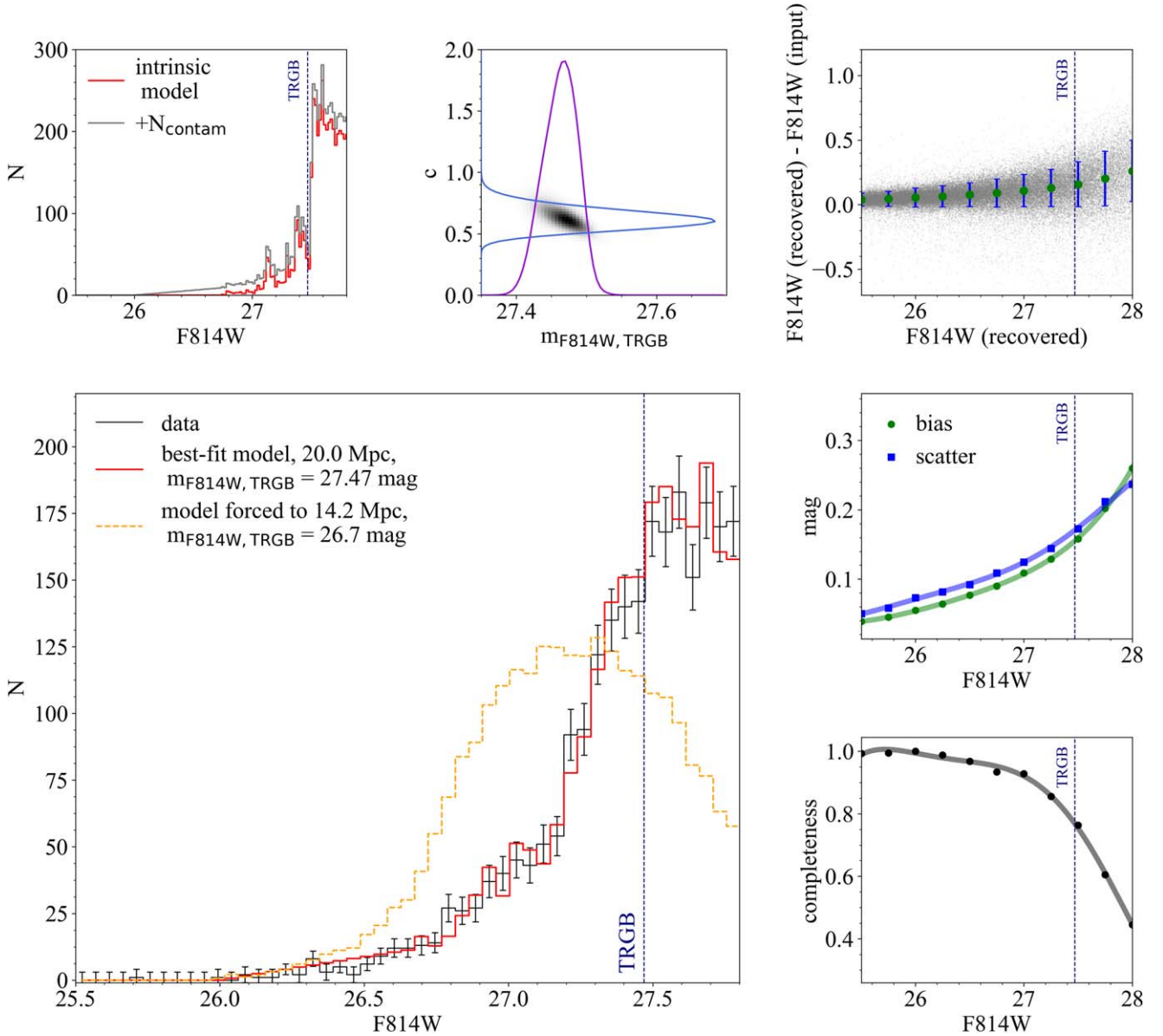
Figure 4. Results from the forward modeling fit to the *I*-band luminosity function. The top left panel shows a luminosity function with a TRGB magnitude of 27.47 mag. Panels on the right show the systematic offset (bias) and the scatter between true and recovered magnitudes using the artificial star test (top and middle), as well as the completeness (bottom). The main panel shows the observed luminosity function (black), as well as the intrinsic model perturbed with the measurement errors (red). This model is an excellent fit. The likelihood is indicated in the central panel of the top row.

adopt the systematic uncertainty on the zero-point calibration from Rizzi et al. (2007) of 0.07 mag which is the standard in the field (see, e.g., McQuinn et al. 2017). Adding this uncertainty in quadrature leads to a final distance modulus of $31.50^{+0.04+0.16+0.07}_{-(0.02+0.16+0.07)} = 31.50 \pm 0.18$ mag and a distance of 20.0 ± 1.6 Mpc.

5. Discussion

In this Letter we have used deep HST/ACS imaging to determine a tip of the red giant branch distance to one of the two dark matter-deficient galaxies in the field of NGC 1052, NGC 1052-DF4. The new data, acquired in Cycle 26 thanks to the midcycle process, comprises seven orbits of F814W and three orbits of F606W imaging. Together with the previously obtained single orbit imaging in both bands the data are just

deep enough to allow detection of individual stars fainter than the TRGB (see Figure 2).

Our best estimate for the distance is 20.0 ± 1.6 Mpc. This result is consistent with the SBF distance (19.9 ± 2.8 Mpc) and the TRGB lower limit (>9.7 Mpc) presented in Cohen et al. (2018) for this galaxy. It is also consistent with the calibration-free SBF distance of 18.7 ± 1.7 Mpc derived in van Dokkum et al. (2018d) for NGC 1052-DF2, with the globular cluster-calibrated SBF distance of 20.4 ± 2.0 Mpc to that galaxy derived by Blakeslee & Cantiello (2018), and with the distance of the elliptical galaxy NGC 1052 (19.2–20.6 Mpc; Tonry et al. 2001; Tully et al. 2013). Our results do not agree with the distance derived by Monelli & Trujillo (2019), who found $m_{F814W,TRGB} = 26.7 \pm 0.1$ and $D_{TRGB} = 14.2 \pm 0.7$ Mpc from the same data that were previously analyzed by Cohen et al. (2018) and van Dokkum et al. (2018d). The best fit when forcing the TRGB magnitude

to the Monelli & Trujillo (2019) value is shown by the broken line in Figure 4. All previous studies used the 1+1 orbits in F814W and F606W from program GO-14644 (PI: van Dokkum). We suggest that a combination of AGB stars and photometrically contaminated giants in these shallow data were incorrectly interpreted as the TRGB by Monelli & Trujillo (2019). Based on the near-identical CMDs of NGC 1052-DF4 and NGC 1052-DF2 we infer that this also happened in the Trujillo et al. (2019) analysis of NGC 1052-DF2 (for more discussion, see van Dokkum et al. 2018d).

Our analysis confirms the unusual nature of NGC 1052-DF4. The spectroscopically confirmed globular clusters of NGC 1052-DF4 rival the most luminous globular clusters in the Milky Way, and its kinematics are consistent with the galaxy having little or no dark matter. The velocity dispersion of the galaxy is $\sigma_{\rm intr} = 4.2^{+4.4}_{-2.2}$ km s^{-1} and the expected value from the stars alone is $\sigma_{\rm stars} \approx 7$ km s^{-1} (see van Dokkum et al. 2019a). High resolution spectroscopy of the diffuse light of NGC 1052-DF4 may provide a more accurate measurement of the kinematics in the future.

Our analysis of the new data places NGC 1052-DF2 and NGC 1052-DF4 at a distance that is consistent, within the errors, with the distance to NGC 1052 itself, at ≈ 20 Mpc.[14] The fact that the group is dominated by an elliptical galaxy is likely important in the context of understanding their formation. Proposed formation scenarios include assembly in the chaotic gas-rich environment of the assembling central galaxy (van Dokkum et al. 2018c), severe tidal stripping (Ogiya 2018; Müller et al. 2019), formation in a QSO outflow from NGC 1052's black hole (Natarajan et al. 1998), and high velocity collisions of gas-rich dwarfs at early epochs (Silk 2019). At minimum, the presence of an overdensity likely influenced the probability of the formation of these galaxies. We note that the confirmation of the distance also confirms the presence of extremely luminous globular clusters in NGC 1052-DF2 and NGC 1052-DF4, and that any formation scenario should account for these objects.

Looking ahead, we also expect a distance measurement for NGC 1052-DF2 in the near future. This galaxy will be imaged with HST in Cycle 27 for 38 orbits, bringing the total exposure time on that galaxy to 20 orbits in F814W and 20 in F606W. These data will be taken in three epochs to help identify the AGB/RGB boundary using stellar variability.

ORCID iDs

Shany Danieli ● https://orcid.org/0000-0002-1841-2252

Pieter van Dokkum ● https://orcid.org/0000-0002-8282-9888
Roberto Abraham ● https://orcid.org/0000-0002-4542-921X
Charlie Conroy ● https://orcid.org/0000-0002-1590-8551
Andrew E. Dolphin ● https://orcid.org/0000-0001-8416-4093
Aaron J. Romanowsky ● https://orcid.org/0000-0003-2473-0369

References

Beaton, R. L., Seibert, M., Hatt, D., et al. 2019, ApJ, 885, 141
Bennet, P., Sand, D. J., Crnojević, D., et al. 2019, ApJ, 885, 153
Blakeslee, J. P., & Cantiello, M. 2018, RNAAS, 2, 146
Blakeslee, J. P., Lucey, J. R., Tonry, J. L., et al. 2002, MNRAS, 330, 443
Caldwell, N. 2006, ApJ, 651, 822
Choi, J., Dotter, A., Conroy, C., et al. 2016, ApJ, 823, 102
Cohen, Y., van Dokkum, P., Danieli, S., et al. 2018, ApJ, 868, 96
Conroy, C., Strader, J., van Dokkum, P., et al. 2018, ApJ, 864, 111
Dalcanton, J. J., Williams, B. F., Lang, D., et al. 2012, ApJS, 200, 18
Dalcanton, J. J., Williams, B. F., Seth, A. C., et al. 2009, ApJS, 183, 67
Danieli, S., van Dokkum, P., Conroy, C., Abraham, R., & Romanowsky, A. J. 2019, ApJL, 874, L12
Dolphin, A. E. 2000, PASP, 112, 1383
Dotter, A. 2016, ApJS, 222, 8
Emsellem, E., van der Burg, R. F. J., Fensch, J., et al. 2019, A&A, 625, A76
Geha, M., Weisz, D., Grocholski, A., et al. 2015, ApJ, 811, 114
Hatt, D., Freedman, W. L., Madore, B. F., et al. 2018, ApJ, 866, 145
Krist, J. 1995, in ASP Conf. Ser. 77, Astronomical Data Analysis Software and Systems IV, ed. R. A. Shaw, H. E. Payne, & J. J. E. Hayes (San Francisco, CA: ASP), 349
Laporte, C. F. P., Agnello, A., & Navarro, J. F. 2019, MNRAS, 484, 245
Lee, M. G., Freedman, W. L., & Madore, B. F. 1993, ApJ, 417, 553
Makarov, D., Makarova, L., Rizzi, L., et al. 2006, AJ, 132, 2729
Martin, N. F., Collins, M. L. M., Longeard, N., & Tollerud, E. 2018, ApJL, 859, L5
McQuinn, K. B. W., Skillman, E. D., Dolphin, A. E., Berg, D., & Kennicutt, R. 2017, AJ, 154, 51
Merritt, A., van Dokkum, P., Abraham, R., & Zhang, J. 2016, ApJ, 830, 62
Monelli, M., & Trujillo, I. 2019, ApJL, 880, L11
Müller, O., Rejkuba, M., & Jerjen, H. 2018, A&A, 615, A96
Müller, O., Rich, R. M., Román, J., et al. 2019, A&A, 624, L6
Natarajan, P., Sigurdsson, S., & Silk, J. 1998, MNRAS, 298, 577
Ogiya, G. 2018, MNRAS, 480, L106
Peacock, M. B., Strader, J., Romanowsky, A. J., & Brodie, J. P. 2015, ApJ, 800, 13
Radburn-Smith, D. J., de Jong, R. S., Seth, A. C., et al. 2011, ApJS, 195, 18
Rizzi, L., Tully, R. B., Makarov, D., et al. 2007, ApJ, 661, 815
Sand, D. J., Spekkens, K., Crnojević, D., et al. 2015, ApJL, 812, L13
Schlafly, E. F., & Finkbeiner, D. P. 2011, ApJ, 737, 103
Silk, J. 2019, MNRAS, 488, L24
Tonry, J. L., Dressler, A., Blakeslee, J. P., et al. 2001, ApJ, 546, 681
Trujillo, I., Beasley, M. A., Borlaff, A., et al. 2019, MNRAS, 486, 1192
Tully, R. B., Courtois, H. M., Dolphin, A. E., et al. 2013, AJ, 146, 86
van Dokkum, P., Cohen, Y., Danieli, S., et al. 2018a, ApJL, 856, L30
van Dokkum, P., Cohen, Y., Danieli, S., et al. 2018b, RNAAS, 2, 54
van Dokkum, P., Danieli, S., Abraham, R., Conroy, C., & Romanowsky, A. J. 2019a, ApJL, 874, L5
van Dokkum, P., Danieli, S., Cohen, Y., et al. 2018c, Natur, 555, 629
van Dokkum, P., Danieli, S., Cohen, Y., Romanowsky, A. J., & Conroy, C. 2018d, ApJL, 864, L18
van Dokkum, P., Danieli, S., Romanowsky, A., Abraham, R., & Conroy, C. 2019b, RNAAS, 3, 29
van Dokkum, P., Wasserman, A., Danieli, S., et al. 2019c, ApJ, 880, 91

---

[14] The distances of other group members are highly uncertain; see van Dokkum et al. (2019b) and Monelli & Trujillo (2019) for a discussion.